Article

Direct-drive photovoltaic electrodialysis via flow-commanded current control

Jonathan Tae-Yoon Bessette ✉, Shane Richard Pratt & Amos G. Winter V

Renewable powered, brackish groundwater desalination is an underutilized resource in the developing world, where there are unreliable energy sources and reliance on increasingly saline groundwater. Traditional renewable desalination technologies require sizable energy storage for sufficient water production, leading to increased cost, maintenance and complexity. We theorize and demonstrate a simple control strategy—flow-commanded current control—using photovoltaic electrodialysis (PV-ED) to enable direct-drive (little to no energy storage), optimally controlled desalination at high production rates. This control scheme was implemented on a fully autonomous, community-scale (2–$5\,\mathrm{m^3\,d^{-1}}$) PV-ED prototype system and operated for 6 months in New Mexico on real brackish groundwater. The prototype fully harnessed 94% of the extracted PV energy despite featuring an energy storage to water productivity ratio of over 99% less than the median PV desalination systems in literature. Flow-commanded current control PV-ED provides a simple strategy to desalinate water for resource-constrained communities and has implications for decarbonizing larger, energy-intensive desalination industries.

Groundwater constitutes 98% of global freshwater sources[1] and 50% of the world's drinking water[2]. Dependence on groundwater is highest in rural areas[1] and in emerging economies[3]. However, the increasing salinity of groundwater, attributed to aridification and climate change[4], poses a growing concern, particularly to low- and middle-income countries[5]. In arid and semi-arid regions, groundwater is commonly the only source of water in spite of widespread salinity beyond permissible drinking limits[2].

Inland brackish water desalination is an underutilized process with potential to provide water to under-served communities. However, it is a challenge to effectively harness saline water in these settings. The majority of current desalination processes focus on large-scale, centralized plants with stable power supplies near ocean coasts. Approximately 84.5% of all desalination is within 50 km of a coast with 61% of that for seawater desalination[6,7]. However, around 60% of the global population lives further than 100 km from the coast[8].

Renewable, brackish water desalination could benefit inland, resource-constrained communities, but current desalination solutions for these communities incur high operating expenditures (OPEX)[9], capital expenditures[10] and complexity due to large, necessary energy storage for high water production[11]. These barriers are especially prevalent at small scales (10–$100\,\mathrm{m^3\,d^{-1}}$) resulting in low adoption despite high demand[12] and decentralized users accounting for 80% of the water stressed population[13]. Eliminating batteries could lower barriers to adoption, however, this poses a challenge due to the limited operating power bandwidth of traditional desalination methods[14,15] and the variable nature of renewable energy technologies.

The current industry standard desalination technology is reverse osmosis (RO), which traditionally operates in stable environments with large, constant power supplies; its inflexible control and high energy consumption renders it challenging to adapt to decentralized desalination[16,17]. RO cannot traditionally tolerate or fully harness power intermittency (such as from renewable energy) without large energy storage capacity. Some literature has shown variable flow control on RO units for power tracking in simulation[18–20], but in practice[21–23], operating constraints[24,25] related to membrane pressure and flux lead to a lack of operating power bandwidth. These variable flow control approaches consequently still require energy storage to operate with intermittencies. Other technologies prevalent in low-income communities include solar-thermal-based methods and atmospheric condensation,

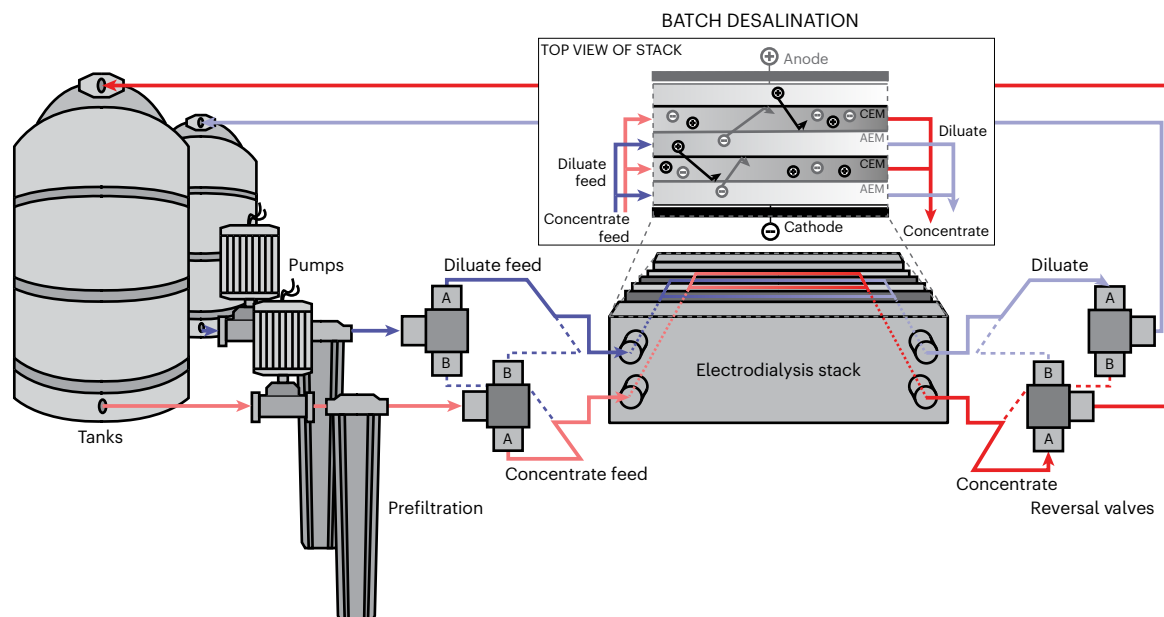Mechanical Engineering, Massachusetts Institute of Technology, Cambridge, MA, USA. ✉e-mail: jbessett@mit.edu

BATCH DESALINATION

Fig. 1 | Conceptual diagram of a batch electrodialysis system. Where water is fed from batch tanks via parallel pumps into optional cartridge filters and then directed through a reversal valve network into the electrodialysis stack. In the electrodialysis stack, ions are transferred across selectively charged membranes: including pairs of a cation exchange membrane (CEM) and anion exchange membrane (AEM). The labels on the valve networks show potential hydraulic pathways, where in this depiction, channel configuration 'A' is engaged and 'B' is disengaged.

but these are commonly limited to household applications with low water productivity[26] (Supplementary Section 1).

The potential of electrodialysis for batteryless operation

Electrodialysis (ED) is an alternative separation technique that has a number of merits relative to RO. ED functions by flowing feed solution through a stack of spacers, each separated by selectively charged cation and anion exchange membranes (Fig. 1). An applied electric field drives the transport of ions across these membranes. The process is operated with either continuous flow of water through the stack or via batches of water recirculating through the stack[27]. This electrically driven—rather than pressure-driven—process causes reduced energy consumption[28] and cost[29] in brackish water and partial desalination scenarios. The energy efficiency of ED reduces solar or wind array sizes and thus capital cost and system footprint. The high water efficiency of ED is especially beneficial in water stressed regions[6]; this feature reduces brine volume, which is often challenging to manage and a relatively large source of operational costs[30]. Moreover, ED exhibits the capability to adjust to changes in feedwater concentration and modify the target output concentration. ED can effectively manage feedwater with higher turbidity, and its membranes can endure exposure to chlorine, commonly utilized for disinfection and antifouling purposes[31]. Notably, ED membrane lifetimes can extend to 10–20+ years and demonstrate resilience to a wide range of pH and temperature fluctuations[32]. These characteristics of ED collectively contribute to a reduction in maintenance and OPEX, proving especially valuable in decentralized, resource-constrained scenarios.

A key feature of ED that makes it well suited for renewable desalination is the ability to operate at variable power levels[33], which can aid in reducing or eliminating the need for energy storage. Power distribution in PV-ED (equation (1a)) is composed of the input power (P_{solar}), the power consumed by pumping water ($P_{hydraulic}$), the electrodialysis stack ($P_{electrodialysis}$) and auxiliary loads ($P_{auxiliary}$). The ED system power consumption may be altered by varying voltage and water flow rate. Equations (1b),(1c) describe the scaling and sensitivity of power, $P_{hydraulic}$ and $P_{electrodialysis}$, to changes in flow rate, Q, and the resulting stack current, i,

from an applied voltage. Power scaling arguments are presented in further detail in Supplementary Section 2. Practical limitations to ED system power range are discussed in Supplementary Section 3.

$$P_{solar} = P_{hydraulic} + P_{electrodialysis} + P_{auxiliary} \quad (1a)$$

$$P_{hydraulic} \propto Q^3 \quad (1b)$$

$$P_{electrodialysis} \propto i^2 \quad (1c)$$

An optimally controlled, direct-drive, batteryless electrodialysis system closely tracks and operates at variable power levels to reduce or eliminate battery capacity while maximizing the water produced for any given power. The water production rate is dictated by the desalination rate. This rate is maximized when applying the maximum current and flow rate to the stack[34]. In batch or recirculating systems, maximizing these parameters ensures the fastest water production. However, in a continuous system, the upper limit of the flow rate is often constrained to achieve a target salinity before exiting the stack in a single pass. These two levers, current and flow rate, are nonlinearly related to overall power consumption, as represented in equations ((1a)–(1c)). For all systems, there is a dynamic constraint on the applied current known as limiting current (also known as diffusion-limited current), i_{lim}. This is the current at which complete salt depletion occurs in the boundary layer adjacent to the membrane and can be modelled as a function of flow rate and salt concentration within the stack. Exceeding limiting current results in water dissociation. Limiting current is described in equation (2), where C_d is the concentration in the diluate (least concentrated) stream, and α and β are empirically determined coefficients which depend primarily on the ED stack, but also can be influenced by water composition.

$$i_{lim} \propto \alpha C_d Q^\beta \quad (2)$$

Despite the features of ED that make it theoretically promising, an optimally controlled, direct-drive, renewable-powered electrodialysis
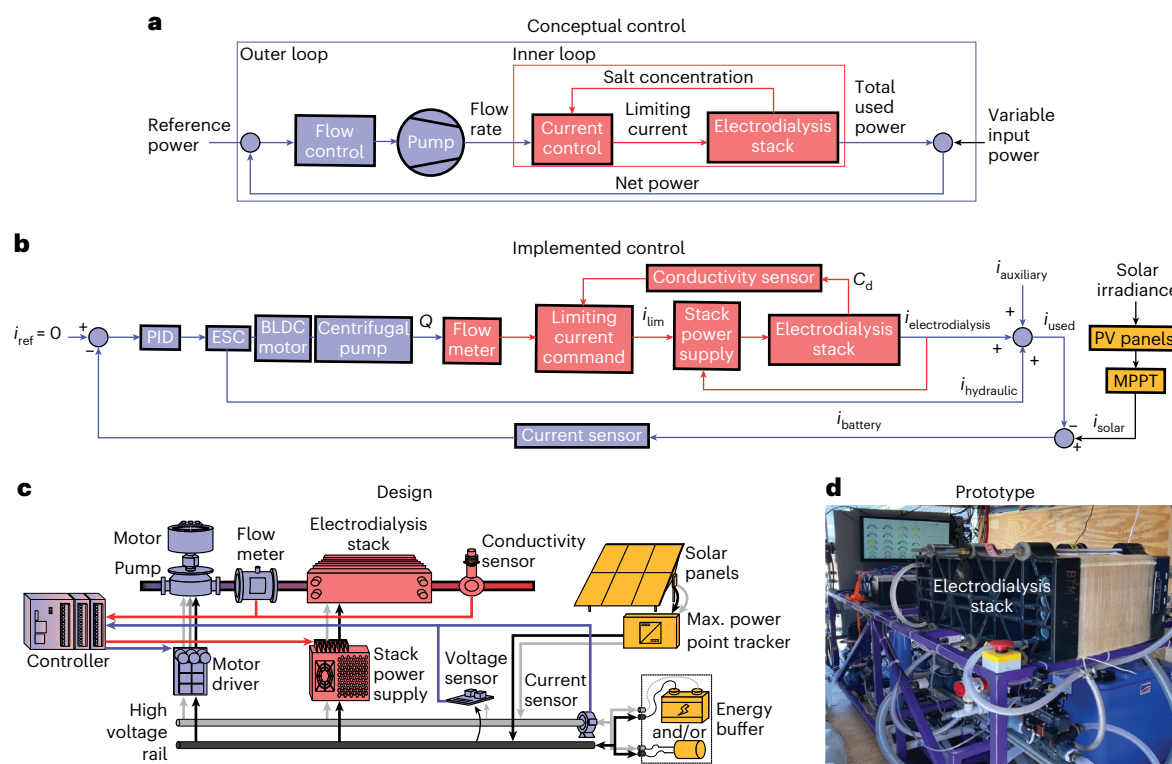
Fig. 2 | Controller design and implementation. a, Conceptual flow-commanded current control (FCCC) block diagram involving cascade control, where the inner loop is used to maximize desalination rate and the outer loop is used for power tracking. Summation operators are intentionally excluded to keep the sign convention generalized, to designer discretion. **b**, Detailed implemented control scheme. **c**, Designed realization of the control strategy on fundamental hardware related to a PV-powered electrodialysis desalination system with colours matching their representative colours in the aforementioned control loops. **d**, Prototype community-scale direct-drive ED system.

system has never been demonstrated in practice without considerable energy storage due to challenges with the control strategy. Variable power ED demonstrations exist but have not achieved both maximal productivity and energy storage reduction in practice; challenges to energy storage reduction include reducing computational speed, accounting for auxiliary loads and mitigating errors accumulated due to controller model inaccuracy. Some researchers have directly coupled the ED stack to photovoltaic (PV) arrays but neglected pump and auxiliary power[35,36]. Other work has examined optimally balancing pumping and stack power but neglected other sources of power consumption[37]. This prior art used predictive, model-based methods to calculate the optimal flow rate and voltage for a given power. However, these methods were too slow relative to solar variability to practically eliminate abrupt power overdraws and thus minimize energy storage; this latency is due to the use of iterative numerical solvers, computationally intensive models and inherent predictive nature. Furthermore, this prior system used voltage control, which required a comprehensive model of the stack resistance updated in real time and an empirically fitted pump model; these models were used to predict power consumption but are hindered by error accumulation from environmental degradation over time. Consequently, both of these models require constant re-calibration. Despite studies concluding PV-ED is a cost-effective solution for brackish water desalination[34–37], these limitations hindered the ability to operate direct-drive practically and with minimal energy storage. Thus, there is a knowledge gap in responsively (rather than predictively) and simply (without complex models) applying direct-drive control to variable power electrodialysis systems.

In this work, we present a responsive, simple control scheme, which enables direct-drive, renewable electrodialysis desalination. We additionally constructed a community-scale pilot system and demonstrated controller robustness and reduction in energy storage in a long-term (6-month) field trial on real groundwater wells in New Mexico amid a variety of solar irradiance and feedwater conditions.

Flow-commanded current control

We propose a simple, responsive control scheme (Fig. 2a) without the need for complex models, which maximizes water production rate while closely aligning with a variable, renewable input power source. This control scheme is described as follows. If the system has surplus power, P_{solar}, it commands (rather than predicts) an increased flow rate and consumes more hydraulic power (equation (1b)). The system then uses current control to apply current to the stack equal to limiting current with a user-determined safety factor. Limiting current is calculated (equation (2)) using simple models[27,38] based solely on flow rate (Q) and diluate conductivity (C_d) measurements. This current command concurrently increases consumed electrical power (equation (1c)). The system continues to increase the flow rate and concurrently and consequently, the applied current density, until the sum of their power has matched the available power (equation (1a)). In the case where the system has a reduction in power, it continues to decrease commanded pumping power, and the resulting current density, u, until it has matched the available power. This direct-drive control scheme operates optimally while theoretically utilizing no energy storage.

The control scheme employs *cascade feedback* control[39]. The use of feedback control greatly increases response speed compared with prior control strategies that used computationally expensive numerical solvers[34,37]. Feed-forward control is an alternative method that could be faster but requires accurate understanding of the plant, which is transient and difficult to accurately model in our case. The cascade control scheme features an inner and outer feedback loop, which maximize desalination rate and track power intermittencies,
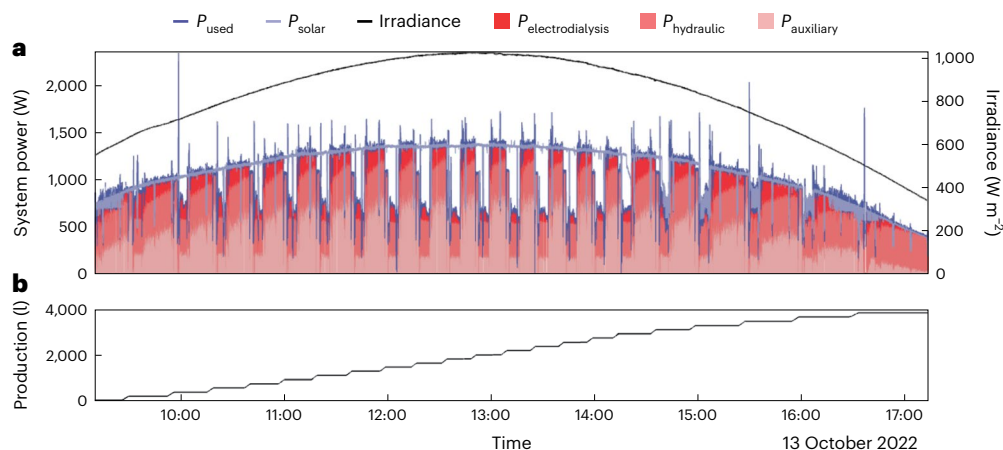
Fig. 3 | Single example day of operation on 13 October 2022. a, Used power tracking solar power in blue overlaid on top of subsystem power distribution in red hues, where the subsystem powers consist of the electrodialysis stack power, the hydraulic power, and the auxiliary power. Solar irradiance is plotted on the right axis. **b**, The aggregate water production, which appears in steps due to batch-operation over the day.

respectively. The outer loop commands changes in flow rate to track power, allowing practical flexibility to changes in power source and auxiliary system power consumption (valves, sensors). The inner loop applies the maximum allowable current using current control rather than voltage control, guaranteeing maximum ionic transfer and thus maximum desalination rate. The model of limiting current involves only multiplication of several values (equation (2)), making it computationally efficient. Using current control circumvents the need to implement a resistance model of the stack, which is often inaccurate with respect to changes over time such as from fouling. Further details are in Supplementary Section 4.

A practical control loop implemented in this study is shown in Fig. 2b. The control loop uses current, $i_{battery}$ to indicate net power usage and track a reference current, i_{ref}, of zero. The battery current is the difference between used current, i_{used} and drawn solar current, i_{solar}. The used current includes the sum of hydraulic, electrodialysis and auxiliary currents ($i_{hydraulic}$, $i_{electrodialysis}$ and $i_{auxiliary}$, respectively). The practical feedback loop includes a proportional-integral-derivative (PID) controller, with control effort fed into an electronic speed controller directing current to a brushless direct current motor for flow rate changes. Solar power is drawn via a maximum power point tracker connected to the photovoltaic (PV) panels.

Whereas operating at higher flow rates increases water production, it also increases the specific energy consumption (SEC). At high flow rates, hydraulic power exponentially increases at a greater rate than the increase in applicable current to the stack (Supplementary Section 2). However, despite this increased SEC, it is always more favourable for a direct-drive system to consume all of the available energy.

Single-day of operation

We fabricated a fully automated, community-scale system using commercially available hardware and integrated the aforementioned flow-commanded current control (FCCC) control strategy (Fig. 2b) to be tested in a field deployment. The system (Fig. 2c,d) was deployed for 6 months, autonomously operating at the Brackish Groundwater National Research Facility (BGNDRF) in Alamogordo, New Mexico, on different wells (feed salinities of ~1,800 μS cm^{-1} and ~4,000 μS cm^{-1} at wells labelled one and three, respectively) to determine the robustness of this theory among variable solar irradiance conditions. The fabrication, control and modelling are described in Methods and Supplementary Section 5–8.

An example day of operation can be seen in Fig. 3. On this day, the system tracked available power with 7.5 W mean error (Fig. 3a) visually noted by the closeness of the used and extracted solar power over time. The minimum system start-up (~700 W) and operating power (~500 W) restrict the start and end time: on this day, approximately 9:00 a.m.–5:15 p.m. In the middle of the day, faster batch times (Fig. 3b) occurred as a result of higher solar irradiance. High solar irradiance led to more extracted solar power, P_{solar}, and the controller consequently commanded higher flow rate and applied current, resulting in increased production rate. The converse effect was observed at the beginning and end of the day, where lower irradiance led to longer batch times and thus slower production rate. This variable operation throughout the day also led to fluctuations in energy distribution between subsystems, where hydraulic pumping and auxiliary power dominate during the edges of the day.

Full operational summary

Throughout the duration of the field trial, the prototype was able to operate in direct drive with minimal energy storage capacity (Fig. 4a) amid a wide range of solar conditions (Fig. 4b) without control system failure. The energy storage capacity required was not strongly correlated to variability in solar irradiance (Supplementary Fig. 6), indicating the control scheme was robust and independent of a variety of solar power fluctuations. The prototype was able to harness 93.74%, on average, of the electrical energy from the solar panels (Fig. 4c) and thus had higher overall energetic efficiency and water productivity than prior art (later discussed in Fig. 6) despite having minimal energy storage. This was accomplished with product salinities consistently below the target of 1,000 μS cm^{-1}, averaging 966 and 962 μS cm^{-1} on wells one and three, respectively.

On wells one and three, the system produced an average of 5.29 and 2.18 m^3 of water per day (Fig. 4e) using 8.35 and 6.54 kWh, resulting in an SEC (Fig. 4d) of 1.58 and 3.65 kWh m^{-3}, respectively. However, SEC was increased by a variety of system defects including internal leakage within the prototype stack. We observed a stack current efficiency (the ratio of the mass transfer to the applied current) of 40% in contrast to the marketed 90%+ (V. Pavlovic, N. Moe, J. Barber, personal communication). Additionally, the system was limited by hydraulic and auxiliary inefficiencies: the ED stack used on average 8% and 19% of the overall energy, with pumping consuming 42% and 37% and auxiliary consumption at 50% and 45%, on wells one and three, respectively. Auxiliary consumption includes the converter losses, the electrode rinse and antiscalant pumps, control and sensing (Supplementary Fig. 6). The pump hydraulic efficiency is the ratio of hydraulic energy out (pressure drop times flow rate) to electrical energy in (current times voltage). The pump hydraulic efficiency was 10% on average due to its variable operation; centrifugal pumps are most commonly designed for fixed
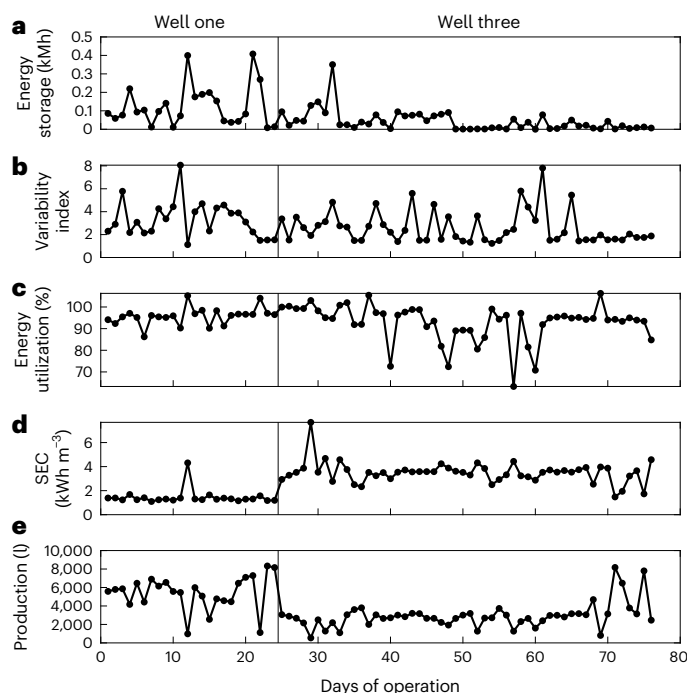
Fig. 4 | Overview of the performance over long-term operation from 4 August 2022 to 9 February 2023. a, Worst-case daily energy storage capacity required. **b**, Variability index, which represents solar irregularity[54]. **c**, Energy utilization, the percent of the available energy harnessed by the system defined as the percentage of used energy to extracted solar energy; in cases where it is above 100%, the used energy exceeded the extracted solar energy and drew excess energy from the battery. **d**, SEC: the energy to produce 1 m³ of desalinated water. **e**, Total water production for the day. Days of inactivity due to insufficient irradiance or maintenance were removed. A vertical line is shown to differentiate days of operation on well one and well three.
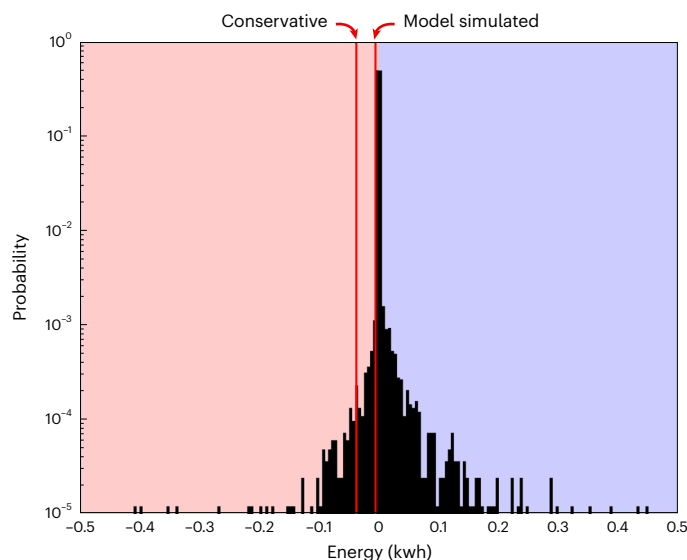

Fig. 5 | Logarithmic histogram showing the field pilot energy discharges and charges required over long-term testing compared with the predicted energy storage requirement. The predicted capacities for the conservative and model-simulated estimate are 0.038 and 0.006 kWh, respectively. The worst-case energetic overshoot over this 6-month time period was 0.408 kWh. The pink shading indicates discharging from the battery and the blue shading indicates charging.

operating conditions. Finally, it should be noted that other direct-drive systems often oversize their solar arrays and run at constant power, thus under-utilizing the available energy; this underutilized energy is not often captured or reported in SEC metrics.

Energy storage reductions

In practice, with commercially available, off-the-shelf components, complete elimination of energy storage is limited by practical considerations including actuator response speed, the control and sensor sampling frequencies and the communication methods. Thus, we conducted system identification on the prototype to estimate the minimum energy storage required (Supplementary Section 8). We used the settling time of slowest dynamic response (the diluate conductivity to changes in current) and our maximum system operating power for a conservative battery sizing estimate (Supplementary Fig. 5f). We additionally constructed a model of the system dynamics to simulate a holistic system response (Supplementary Figs. 4 and 5). The energy storage identified for conservative and model-simulated sizing methodologies were 0.038 and 0.006 kWh, respectively. When compared to our long-term data (Fig. 5), both the model-simulated and conservative battery sizing estimates support the majority of power variability seen in our field trial, covering 99.8% and 99.3% of discharges, respectively; this means our simple energy storage sizing method for FCCC covers nearly all of the power mismatches in practice. On the basis of these predictions, we ran the system on a 0.12 kWh DeWalt drill battery for several days without failure. The drill battery was oversized but low cost, widely available and had an appropriate current rating.

The ratio of battery capacity to production rate and battery capacity to rated system power of this prototype is shown in contrast to prior

PV-RO and PV-ED systems in Fig. 6. Figure 6 was compiled using multiple review papers[10,24,40–45] with additional investigations into their source materials (further detailed in Supplementary Table 3).

The ratio of energy storage to operating power for FCCC PV-ED is 0.015 kWh kW⁻¹. The ratio of energy storage to operating productivity is 0.013 and 0.022 kWh (m³ d⁻¹)⁻¹ for well one and well three, respectively. Direct-drive PV-ED using FCCC uses 99.8% less battery per rated power and over 99.6% less battery per production rate than the median PV desalination systems in literature (7 kWh kW⁻¹ and 3.9 kWh (m³ d⁻¹)⁻¹, respectively). These results support the hypothesis that implementing this control scheme results in a negligible fraction of energy storage, whereas still achieving high productivity compared to literature, enabling practical, batteryless renewable desalination.

Our experimental system architecture had a levelized cost of water of US$6.37 m⁻³ and US$10.89 m⁻³ for wells one and three, assuming a conservative system lifetime of 10 years, with a 40% efficient electrodialysis stack, using off-the-shelf components at retail price (Supplementary Table 2). For reference, <20 m³ d⁻¹ on-grid brackish water RO systems are US$5.6–12.9 m⁻³ (ref. 45) and literature reports PV-RO at US$11.7–15.6 m⁻³ (ref. 46) and PV-ED at US$10.4–11.7 m⁻³ (ref. 47), without commercial markup. This shows we can achieve cost competitive, high-productivity desalination with the added feature of minimal to no batteries using ED (reducing maintenance and increasing adaptability). Furthermore, there is room for system cost reduction via optimization, architectural simplification and economies of scale, as our prototype was designed to demonstrate the controller rather than minimize cost.

Discussion

We created and validated a new, simple control scheme that enables direct-drive electrodialysis desalination with variable power such as renewables. The scheme was implemented on a fully automated system and shown to track power closely enough such that energy storage less than 0.069 kWh (smaller than a drill battery) was sufficient to run a 4.5-kW rated system.

Similarly sized, brackish water, 'batteryless' RO systems report requiring using some small batteries for the maintenance of controls
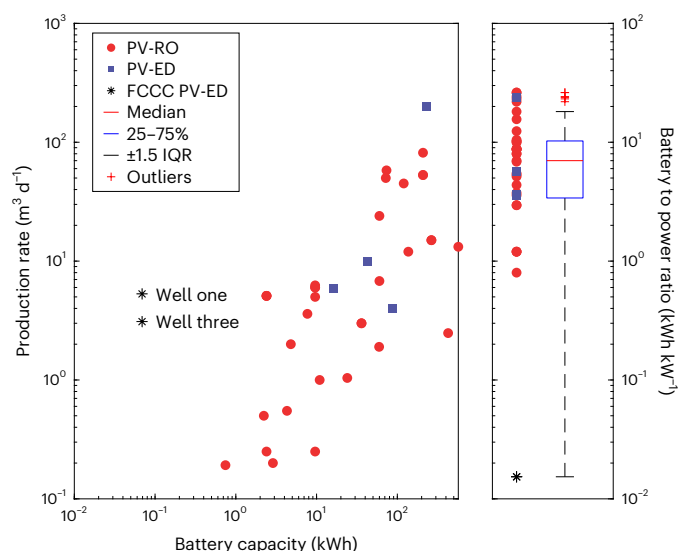
Fig. 6 | Comparison of batteryless, direct-drive FCCC PV-ED to PV-RO and PV-ED systems in prior art. a, Logarithmic plot of daily production rates and associated battery capacities. For increasing production rate or larger systems, larger energy storage is often needed for traditional systems in contrast to FCCC PV-ED. **b**, Logarithmic dot and boxplot of battery to rated system power ratios. FCCC PV-ED is lower in energy storage to rated system power ratio than literature (refs. 10,24,40–45).

and sensing[10,24,40–45]. The minimum energy storage of this prototype is comparable to or smaller than what is reported in these studies; our prototype's energy storage can thus be considered negligible and comparable in size to state of the art 'batteryless' (direct-drive) reverse osmosis systems. The prototype additionally featured a battery capacity to water production ratio over 99% less than the median value existent in literature, indicating high production rates despite little energy storage. This advancement enables an entirely different operating scheme than presented in prior art—a reactive, rather than predictive, ED control technique without complex models—allowing immediate variable power tracking and reducing battery capacity.

FCCC could also be applied to directly link variable power sources to other emerging electrochemical membrane applications (for example, selective ED for agriculture, high temperature and high salinity ED for produced water from oil and gas, bipolar membrane ED for carbon capture, electrodeionization for ultra-pure water in semiconductors and field hospitals and potentially even fuel cells for hydrogen production. Finally, the utility of FCCC PV-ED as a partial desalination step before large-scale RO plants could also be investigated in future work.

A limitation of this work is that the effectiveness of FCCC and subsequent battery capacity required depend on the system components chosen. Actuators, including the electrodialysis stack power supply and the pumps, must be sized appropriately with respect to the energy source to utilize the desired range of power variability. For instance, an undersized pump may not capture the full bandwidth of power but would be less expensive. However, incorporating a slightly larger pump could enable exponentially greater power tracking bandwidth (equation (1b)) for a marginal increase in cost.

The long-term field test under authentic solar and challenging groundwater conditions presented herein demonstrates that FCCC can bridge the gap between renewable energy sources and desalination, enabling high production, batteryless, sustainable desalination. This work has the potential to broaden the reach of desalination to resource-constrained communities worldwide while also providing a catalyst for larger industrial desalination plants to economically decarbonize.

Methods

System fabrication

We constructed a fully automated, batch electrodialysis desalination system using commercially available hardware based on optimization from ref. 48 for a community-scale application but incorporated modified controls (Fig. 2b), sensing (Supplementary Table 1), communication and improved hydraulic architecture to implement and test FCCC (Fig. 2d and Supplementary Fig. 2). A community-scale system size was chosen to meet the requirements of humanitarian crises and remote development scenarios[49] and is a size the authors have prior experience piloting.

We integrated a smaller footprint (relative to industrial plants), high production rate, commercially available stack (SUEZ WTS V20 prototype stack (2022) with 150 cell pairs) to test the control scheme. The stack contained capacitive carbon electrodes[50,51], which reached charge saturation at approximately 80,000 coulombs. Our reversal mechanism was triggered if we reached this saturation threshold. However, we sized the batch tank volumes to reverse only between batches; reversing during the middle of a batch would cause remixing of high and low salt concentrations in the tanks, decreasing the energy efficiency. Reversing after every batch completion still results in partial remixing of solutions because of residual concentrate and diluate within the stack and piping; these losses can be avoided with shorter pipes, smaller stacks, cone- rather than flat-bottom tanks and by considering reversals after a series of batches. This prospect is possible with conventional metal electrodes (which do not reach charge saturation and rather operate with Faradaic reactions). However, reversing less frequently also creates more potential for fouling. The batch volumes in our pilot system were consequently designed to be 300 l as a function of our feed and target salinities. We additionally used equal sized diluate and concentrate batch volumes with conservative recovery (50%) relative to the capabilities of ED for convenience, however, it is common to run ED systems at higher recoveries (up to 95% (ref. 27)). The capacitive electrodes facilitated the use of feed salinity as the electrode rinse, which was periodically fed and drained via solenoid valves.

The remaining components were sized based on the stack chosen. The two pumps (3SV4GA30 Xylem Goulds Multistage centrifugal) were sized according to the stack flow rate ranges. The power electronics were sized according to the stack voltage and current ranges. The solar panels were sized to provide the maximum actuator (pumps and stack power supply) power at peak irradiance. We thus integrated six 280-W solar panels (SolaRover) available at BGNDRF. Two 1.2-kWh batteries were connected for maintenance and code adjustment during hours in which solar was unavailable; their size was chosen out of convenience and availability of old laboratory hardware. A 120-Wh drill battery (DeWalt) was used for demonstrating the minimal energy storage required by the direct-drive control scheme; its size was chosen based on the system identification and modelling conducted (Supplementary Figs. 4 and 5).

Our prefiltration architecture was also designed to meet requirements set by the stack manufacturer. This architecture included cartridge sediment filters and ion-exchange resin cartridges (iSpring FM25B) for removing >5-μm particles and producing <5 mg l^{-1} iron. On well three, we dosed approximately 14 ml per batch of antiscalant (SUEZ Hypersparse MDC776).

A full process and interface diagram including more details on system design can be found in the supplement (Supplementary Fig. 2) to the interested reader. These include additional sensors, the communication network for remote monitoring and any additional component specifications (Supplementary Table 1).

Controller integration

Both control loops (inner and outer loop) were implemented on a Koyo Click PLC, chosen for its low cost, familiarity to industry

practitioners and simple ladder logic programming structure. We additionally employed a higher-level state machine (Supplementary Table 1) within the PLC main programme, incorporating some insights from refs. 34,48 for managing the batch states, errors and system start-up and nighttime shutdown.

The inner loop sensing scheme was implemented with an inductive flow meter (ProSense FMM100-1001) placed immediately before the stack inlet and toroidal conductivity meter (Sensorex TCS3020) placed directly after the desalination stack on the diluate stream. Both are read over Modbus TCP to the PLC at 100 Hz sampling frequency. A subroutine was built to determine and command limiting current using pre-programmed constants (α, β from equation (2)) based on stack geometry, spacer, membrane and solution characteristics. Using the constructed system and feedwater, we acquire α and β by measuring the limiting current at various flow rate and conductivity conditions following methodology from ref. 38. However, many other methods for modelling limiting current exist.

The limiting current equation was fit within 0.22 A root mean squared error of the actual identified limiting current values; the equation was fitted to the full operational range of flow rates and input salinities at our field site (Supplementary Fig. 3). The validity of the empirically fit limiting current equation should be considered in the context of the application; an application with wide ranges in salinity, pH and changes in composition may have worse accuracy to the fit equation. If these regions are not within the safety factor applied, over-limiting current may be applied. Solutions to avoid over-limiting current include larger safety factors, adjusting the equation to account for component compositions or superposition of multiple limiting current models. Limitations also include the need to empirically identify α and β parameters, however, there are values in literature that generally fit a variety of stack sizes and behaviours[38].

The outer loop PID was implemented by using a built-in function within the PLC to track an analogue hall effect current sensor (Chen Yang CYHCT-C3TC) placed on the positive lead of the battery terminal, with a setpoint of zero; any current into the battery would indicate excess solar power and lead to an increase in pump speed. Any current out of the battery would indicate system overdraws and ramp down the pump speeds. A voltage sensor was considered but was not high enough in resolution given the relatively flat voltage–charge curve of a lithium ion phosphate battery; voltage sensors, however, could be better suited for capacitor banks or when using an integrated controller-maximum power point tracker architecture.

We set the PID constants by first using the operating bandwidth to determine integral gain heuristically[52]; these equations are detailed in Supplementary Section 5. We then increased the proportional gain until we observed instability and reduced it by a factor of safety from the unstable gain point. The tuned PID gains were $K_p = 10$, $K_i = 1$ and $K_d = 0$ (proportional, integral and zero derivative gain, respectively). This tracking was stable throughout all days of operation. Figures regarding the tuning can be found in the supplement. The outer loop is for power tracking and is not limited solely to PID control; other methods (for example, nonlinear, on–off) may be implemented. Feedback controller PID tuning using heuristics is useful for ease of operator implementation, but many alternative methods including frequency domain loop shaping, pole-zero cancellation and so on can be employed depending on user requirements.

System identification and modelling

Using the constructed system, we conducted system identification on the hydraulic and stack dynamics using step responses on the pump speed and stack current commands (Supplementary Fig. 5a–d). We aimed to construct (1) a simple, conservative battery estimate using the longest system settling time and maximum system power and (2) an estimate using a simulation-based construction (MathWorks Simulink). Feedwater from well three was utilized for the system identification.

The longest settling time was the stack conductivity response to current changes (approximately 30 s) and was multiplied by the maximum system power (4,500 W) to determine the energy capacity required (0.038 kWh) (Supplementary Fig. 5f). The simulation-based construction used four plants that were identified: the hydraulic flow rate and power response to pump speed commands and the conductivity and power response to stack current commands (Supplementary Fig. 4). These plants were incorporated with a PID and associated time delays to simulate the overall system response. The overshoot from the step down (Supplementary Fig. 5e) was greater than the step up, and the energy associated with this worst-case overshoot from the step down was utilized to predict the energy capacity required (0.006 kWh).

Data availability

Source data are available via Figshare at https://doi.org/10.6084/m9.figshare.24991158 (ref. 53).

References

1. *United Nations World Water Development Report 2022: Groundwater: Making the Invisible Visible* (UNESCO, 2022).
2. Margat, J. & Van der Gun, J. *Groundwater Around the World: A Geographic Synopsis* (CRC Press, 2013).
3. Thomas, B., Vinka, C., Pawan, L. & David, S. Sustainable groundwater treatment technologies for underserved rural communities in emerging economies. *Sci. Total Environ.* **813**, 152633 (2022).
4. Kaushal, S. S. et al. Freshwater salinization syndrome: From emerging global problem to managing risks. *Biogeochemistry* **154**, 255–292 (2021).
5. Vineis, P., Chan, Q. & Khan, A. Climate change impacts on water salinity and health. *J. Epidemiol. Glob. Health* **1**, 5–10 (2011).
6. Jones, E., Qadir, M., van Vliet, M. T., Smakhtin, V. & Kang, S.-m The state of desalination and brine production: a global outlook. *Sci. Total Environ.* **657**, 1343–1356 (2019).
7. Eke, J., Yusuf, A., Giwa, A. & Sodiq, A. The global status of desalination: an assessment of current desalination technologies, plants and capacity. *Desalination* **495**, 114633 (2020).
8. Griggs, G. *Coasts in Crisis: A Global Challenge* (Univ. of California Press, 2017).
9. Rezk, H. et al. Fuel cell as an effective energy storage in reverse osmosis desalination plant powered by photovoltaic system. *Energy* **175**, 423–433 (2019).
10. Abdelkareem, M. A., Assad, M. E. H., Sayed, E. T. & Soudan, B. Recent progress in the use of renewable energy sources to power water desalination plants. *Desalination* **435**, 97–113 (2018).
11. Seetharaman, K. M., Nitin Patwa, S. & Gupta, Y. Breaking barriers in deployment of renewable energy. *Heliyon* **5**, e01166 (2019).
12. Song, J., Li, T., Wright-Contreras, L. & Law, A. W.-K. A review of the current status of small-scale seawater reverse osmosis desalination. *Water Int.* **42**, 618–631 (2017).
13. *Sustainable Development Report* (United Nations, 2022).
14. Mito, M. T., Ma, X., Albuflasa, H. & Davies, P. A. Reverse osmosis (RO) membrane desalination driven by wind and solar photovoltaic (PV) energy: state of the art and challenges for large-scale implementation. *Renew. Sustain. Energy Rev.* **112**, 669–685 (2019).
15. Shokri, A. & Fard, M. S. Water–energy nexus: cutting edge water desalination technologies and hybridized renewable-assisted systems; challenges and future roadmaps. *Sustain. Energy Technol. Assess.* **57**, 103173 (2023).
16. Ghaffour, N., Bundschuh, J., Mahmoudi, H. & Goosen, M. F. Renewable energy-driven desalination technologies: a comprehensive review on challenges and potential applications of integrated systems. *Desalination* **356**, 94–114 (2015).

17. Alawad, S. M., Mansour, R. B., Al-Sulaiman, F. A. & Rehman, S. Renewable energy systems for water desalination applications: a comprehensive review. *Energy Convers. Manage.* **286**, 117035 (2023).

18. Miranda, M. S. & Infield, D. A wind-powered seawater reverse-osmosis system without batteries. *Desalination* **153**, 9–16 (2003).

19. Thomson, M. & Infield, D. A photovoltaic-powered seawater reverse-osmosis system without batteries. *Desalination* **153**, 1–8 (2003).

20. Kumarasamy, S., Narasimhan, S. & Narasimhan, S. Optimal operation of battery-less solar powered reverse osmosis plant for desalination. *Desalination* **375**, 89–99 (2015).

21. Thomson, M. & Infield, D. Laboratory demonstration of a photovoltaic-powered seawater reverse-osmosis system without batteries. *Desalination* **183**, 105–111 (2005).

22. Abbasi, N., Ebadi, M. & Khalili, M. Experimental investigation on a standalone battery-less single-phase photovoltaic desalination system. *Int. J. Energy Res.* **46**, 14964–14978 (2022).

23. Mowafy, A. G. & Steiks, I. Direct driven photovoltaic-reverse osmosis hybrid membrane system. In *2022 IEEE 63th International Scientific Conference on Power and Electrical Engineering of Riga Technical University (RTUCON)* 1–9 (IEEE, 2022).

24. Ghermandi, A. & Messalem, R. Solar-driven desalination with reverse osmosis: the state of the art. *Desalin. Water Treat.* **7**, 285–296 (2009).

25. Mito, M. T., Ma, X., Albuflasa, H. & Davies, P. A. Variable operation of a renewable energy-driven reverse osmosis system using model predictive control and variable recovery: towards large-scale implementation. *Desalination* **532**, 115715 (2022).

26. Ahmadi, E., McLellan, B., Ogata, S., Mohammadi-Ivatloo, B. & Tezuka, T. An integrated planning framework for sustainable water and energy supply. *Sustainability* **12**, 4295 (2020).

27. Strathmann, H. Electrodialysis, a mature technology with a multitude of new applications. *Desalination* **264**, 268–288 (2010).

28. Patel, C. G., Barad, D. & Swaminathan, J. Desalination using pressure or electric field? A fundamental comparison of RO and electrodialysis. *Desalination* **530**, 115620 (2022).

29. Patel, S. K., Lee, B., Westerhoff, P. & Elimelech, M. The potential of electrodialysis as a cost-effective alternative to reverse osmosis for brackish water desalination. *Water Res.* **250**, 121009 (2023).

30. Panagopoulos, A., Haralambous, K.-J. & Loizidou, M. Desalination brine disposal methods and treatment technologies-a review. *Sci. Total Environ.* **693**, 133545 (2019).

31. Al-Abri, M. et al. Chlorination disadvantages and alternative routes for biofouling control in reverse osmosis desalination. *npj Clean Water* **2**, 2 (2019).

32. Sedighi, M., Usefi, M. M. B., Ismail, A. F. & Ghasemi, M. Environmental sustainability and ions removal through electrodialysis desalination: operating conditions and process parameters. *Desalination* **549**, 116319 (2023).

33. Campione, A. et al. Coupling electrodialysis desalination with photovoltaic and wind energy systems for energy storage: dynamic simulations and control strategy. *Energy Convers. Manage.* **216**, 112940 (2020).

34. He, W. et al. Voltage-and flow-controlled electrodialysis batch operation: flexible and optimized brackish water desalination. *Desalination* **500**, 114837 (2021).

35. Ortiz, J. M. et al. Electrodialysis of brackish water powered by photovoltaic energy without batteries: direct connection behaviour. *Desalination* **208**, 89–100 (2007).

36. Ortiz, J. et al. Desalination of underground brackish waters using an electrodialysis system powered directly by photovoltaic energy. *Solar Energy Mater. Solar Cells* **92**, 1677–1688 (2008).

37. He, W. et al. Flexible batch electrodialysis for low-cost solar-powered brackish water desalination. *Nat. Water* **2**, 370–379 (2024).

38. Wright, N. C., Shah, S. R. & Amrose, S. E. et al. A robust model of brackish water electrodialysis desalination with experimental comparison at different size scales. *Desalination* **443**, 27–43 (2018).

39. Franks, R. & Worley, C. Quantitative analysis of cascade control. *Ind. Eng. Chem.* **48**, 1074–1079 (1956).

40. Al-Karaghouli, A., Renne, D. & Kazmerski, L. L. Technical and economic assessment of photovoltaic-driven desalination systems. *Renew. Energy* **35**, 323–328 (2010).

41. Ali, M. T., Fath, H. E. & Armstrong, P. R. A comprehensive techno-economical review of indirect solar desalination. *Renew. Sustain. Energy Rev.* **15**, 4187–4199 (2011).

42. Fernandez-Gonzalez, C., Dominguez-Ramos, A., Ibañez, R. & Irabien, A. Sustainability assessment of electrodialysis powered by photovoltaic solar energy for freshwater production. *Renew. Sustain. Energy Rev.* **47**, 604–615 (2015).

43. Shalaby, S. Reverse osmosis desalination powered by photovoltaic and solar rankine cycle power systems: a review. *Renew. Sustain. Energy Rev.* **73**, 789–797 (2017).

44. Hamdan, H., Saidy, M., Alameddine, I. & Al-Hindi, M. The feasibility of solar-powered small-scale brackish water desalination units in a coastal aquifer prone to saltwater intrusion: a comparison between electrodialysis reversal and reverse osmosis. *J. Environ. Manage.* **290**, 112604 (2021).

45. Que, V. N. X., Van Tuan, D., Huy, N. N. & Le Phu, V. Design and performance of small-scale reverse osmosis desalination for brackish water powered by photovoltaic units: a review. *IOP Conf. Ser.: Earth Environ. Sci.* **652**, 012024 (2021).

46. Gorjian, S. & Ghobadian, B. Solar desalination: a sustainable solution to water crisis in Iran. *Renew. Sustain. Energy Rev.* **48**, 571–584 (2015).

47. Manju, S. & Sagar, N. Renewable energy integrated desalination: a sustainable solution to overcome future fresh-water scarcity in India. *Renew. Sustain. Energy Rev.* **73**, 594–609 (2017).

48. Connors, G. B. *Predictive Time-variant Photovoltaic Electrodialysis Reversal: A Novel Design Optimization Using Predictive Machine Learning and Control Theory.* MSc thesis, Massachusetts Institute of Technology (2021).

49. Bessette, J. T. & Winter, A. G. The need for desalination in humanitarian crises. In *Proc. ASME 2022 International Design Engineering Technical Conferences and Computers and Information in Engineering Conference* (ASME, 2022).

50. Barber, J., MacDonald, R., Yang, H. & Lu, W. Capacitive carbon electrodes for electrodialysis reversal applications. In *AWWA/AMTA Membrane Technology Conference* (American Water Works Association, 2014).

51. Campione, A. et al. Water desalination by capacitive electrodialysis: experiments and modelling. *Desalination* **473**, 114150 (2020).

52. Trumper, D. *Control of Mechatronic Systems* (Massachusetts Institute of Technology, 2023); https://trumper.mit.edu/continuous-time-control-control-intro-and-pid

53. Bessette, J. T.-Y., Pratt, S. R. & Winter, A. G. Dataset title. *Figshare* https://doi.org/10.6084/m9.figshare.24991158 (2024).

54. Stein, J., Hansen, C. & Reno, M. J. *The Variability Index: A New and Novel Metric for Quantifying Irradiance and PV Output Variability* number SAND2012-2088C (World Renewable Energy Forum, 2012).

Acknowledgements

Author contributions

J.T.-Y.B. and S.R.P. conceived the idea. J.T.-Y.B. and A.G.W. designed the research. J.T.-Y.B. and S.R.P. carried out the experiment. J.T.-Y.B. performed the data processing and analysis. J.T.-Y.B. and A.G.W. participated in the discussion and writing of the paper.

Competing interests

J.T.-Y.B., S.R.P. and A.G.W. have filed a utility patent application (PCT/US23/29089) based on this work. This intellectual property has potential to be licensed by members of A.G.W.'s research group to start a company.

Additional information

Supplementary information The online version contains supplementary material available at https://doi.org/10.1038/s44221-024-00314-6.

Correspondence and requests for materials should be addressed to Jonathan Tae-Yoon Bessette.

Peer review information *Nature Water* thanks Andrea Cipollina and Xiang-Yu Kong for their contribution to the peer review of this work.

Reprints and permissions information is available at www.nature.com/reprints.

Publisher's note Springer Nature remains neutral with regard to jurisdictional claims in published maps and institutional affiliations.